Journal of Geophysical Research: Biogeosciences

Supporting Information for

Informing Robust Functional Relationship Benchmarks: An Evaluation of the Temperature Sensitivity of Ecosystem Respiration Across the Arctic-Boreal Region

Jeralyn Poe[1], Deborah Huntzinger[1,2,3], William J. Riley[4], Jon M. Wells[5], Edward A. G. Schuur[3], Christopher Schwalm[6], Logan T. Berner[1], Heidi Rodenhizer[6], Nicholas J. Bouskill[7], Victor Brovkin[8], Eleanor J. Burke[9], Philippe Ciais[10], Goran Georgievski[8], Adrian Gustafson[11], David M. Lawrence[12], Andrew H. MacDougall[13], Zelalem A. Mekonnen[4], Joe R. Melton[14], Gesa Meyer[14], Alexandra Pongracz[11], Chunjing Qiu[15], Benjamin N. Sulman[16], Sean C. Swenson[12], Jing Tao[4], David Wårlind[11], Yi Xi[10], Fengming Yuan[16], Qing Zhu[4], and Christina Schädel[6]

[1]School of Informatics, Computing, and Cyber Systems, Northern Arizona University, Flagstaff, AZ, United States of America
[2]School of Earth and Sustainability, Northern Arizona University, Flagstaff, AZ, United States of America
[3]Center for Ecosystem Science and Society, Northern Arizona University, Flagstaff, AZ, United States of America
[4]Climate and Ecosystem Sciences Division, Lawrence Berkeley National Laboratory, Berkeley, CA, United States of America
[5]Department of Soil and Environmental Sciences, University of Wisconsin-Madison, Madison, WI, United States of America
[6]Woodwell Climate Research Center, Falmouth, MA, United States of America
[7]Department of Biological and Ecological Engineering, Oregon State University, Corvallis, OR, United States of America
[8]Department of Climate Dynamics, Max Planck Institute for Meteorology, Hamburg, Germany
[9]Met Office Hadley Centre, Exeter, United Kingdom
[10]Laboratoire des Sciences du Climat et de l'Environnement, CEA-CNRS-UVSQ, Université Paris-Saclay, Gif-sur-Yvette, France
[11]Department of Physical Geography and Ecosystem Science, Lund University, Lund, Sweden
[12]CGD, NSF National Center for Atmospheric Research, Boulder, CO, United States of America
[13]Department of Earth & Environmental Science, St. Francis Xavier University, Antigonish, Canada
[14]Climate Processes Section, Climate Research Division, Environment and Climate Change Canada, Victoria, BC, Canada
[15]Research Center for Global Change and Ecological Forecasting, School of Ecological and Environmental Sciences, Institute of Eco-Chongming, East China Normal University, Shanghai, China
[16]Environmental Sciences Division, Oak Ridge National Laboratory, Oak Ridge, TN, United States of America

Contents of this file

Figures S1 to S11

Tables S1 to S6

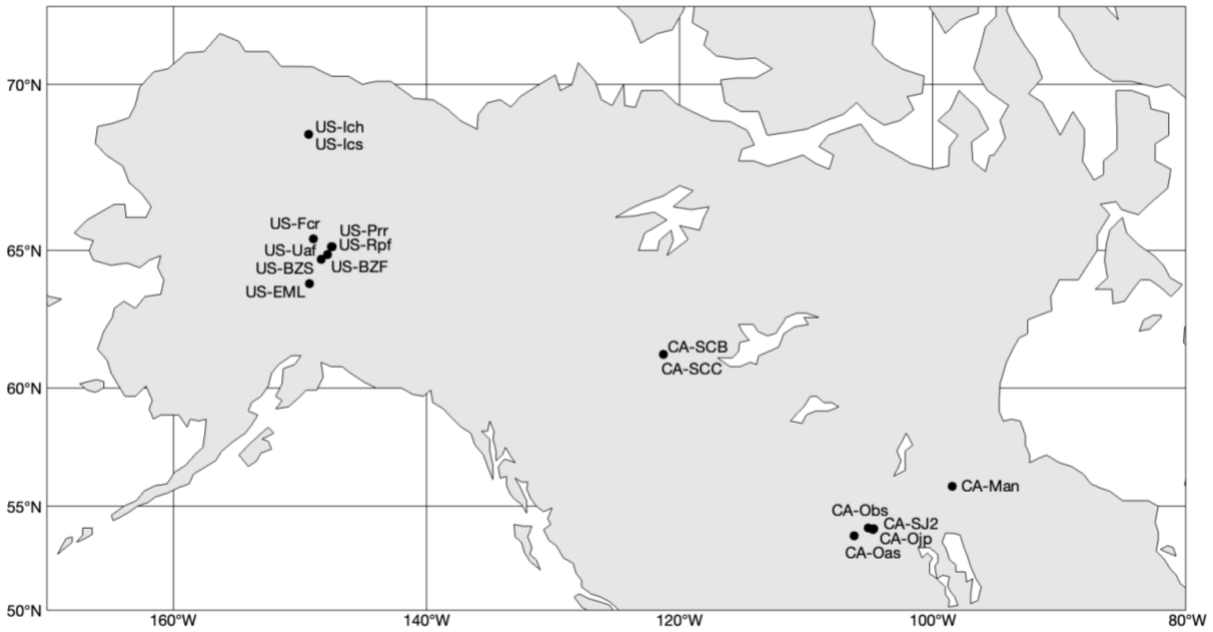


Figure S1. Site map for the 16 flux towers used in the analysis.

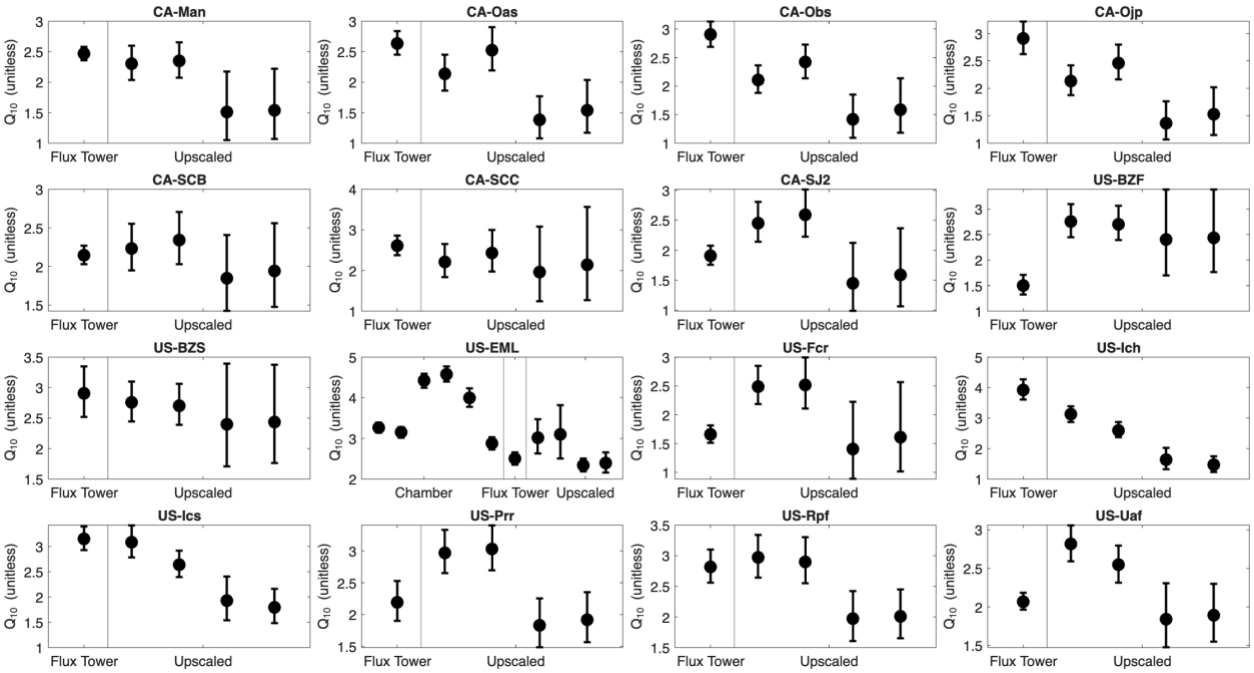


Figure S2. Spread in Q_{10} according to the choice and spatial scale of dataset at each flux tower site. Chamber measurements were only available at US-EML and were calculated from six control plots at CiPEHR. The upscaled category consists of four Q_{10} values calculated from FLUXCOM-X with MERRA-2 and ERA-5 (left) and from Virkkala et al. 2024 with MERRA-2 and ERA-5 (right). Vertical bars indicate the 95% CI of each Q_{10}.

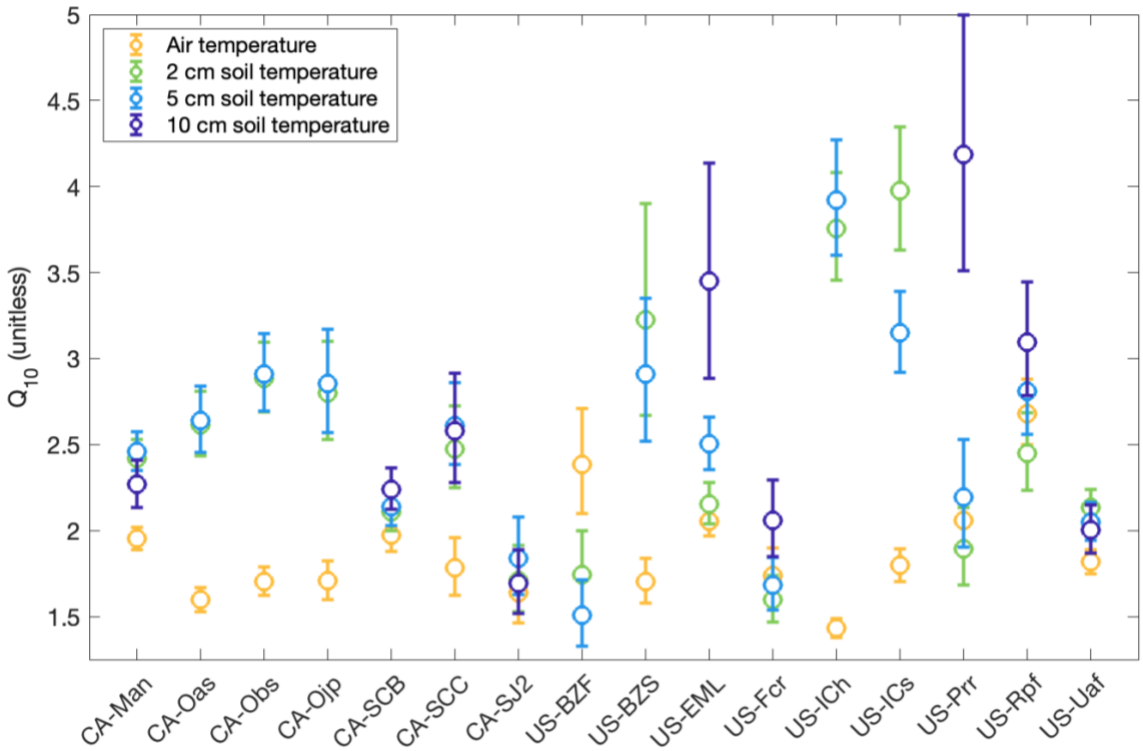


Figure S3. Q_{10} calculated with various soil temperature depths at each flux tower site. Error bars indicate the 95% CI of each Q_{10}. Note that soil temperature at a depth of 10 cm was only available at nine sites.

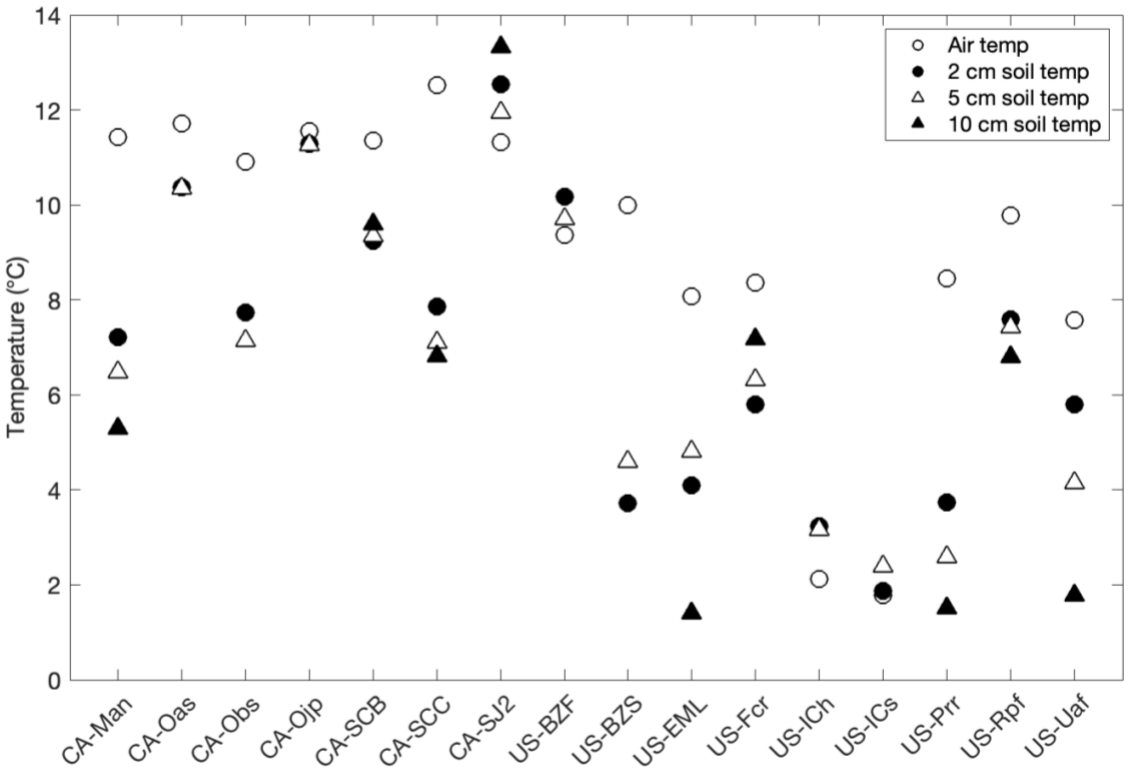


Figure S4. Mean temperature at each depth calculated over the time range available at each flux tower site. Note that soil temperature at a depth of 10 cm was only available at 9 sites.

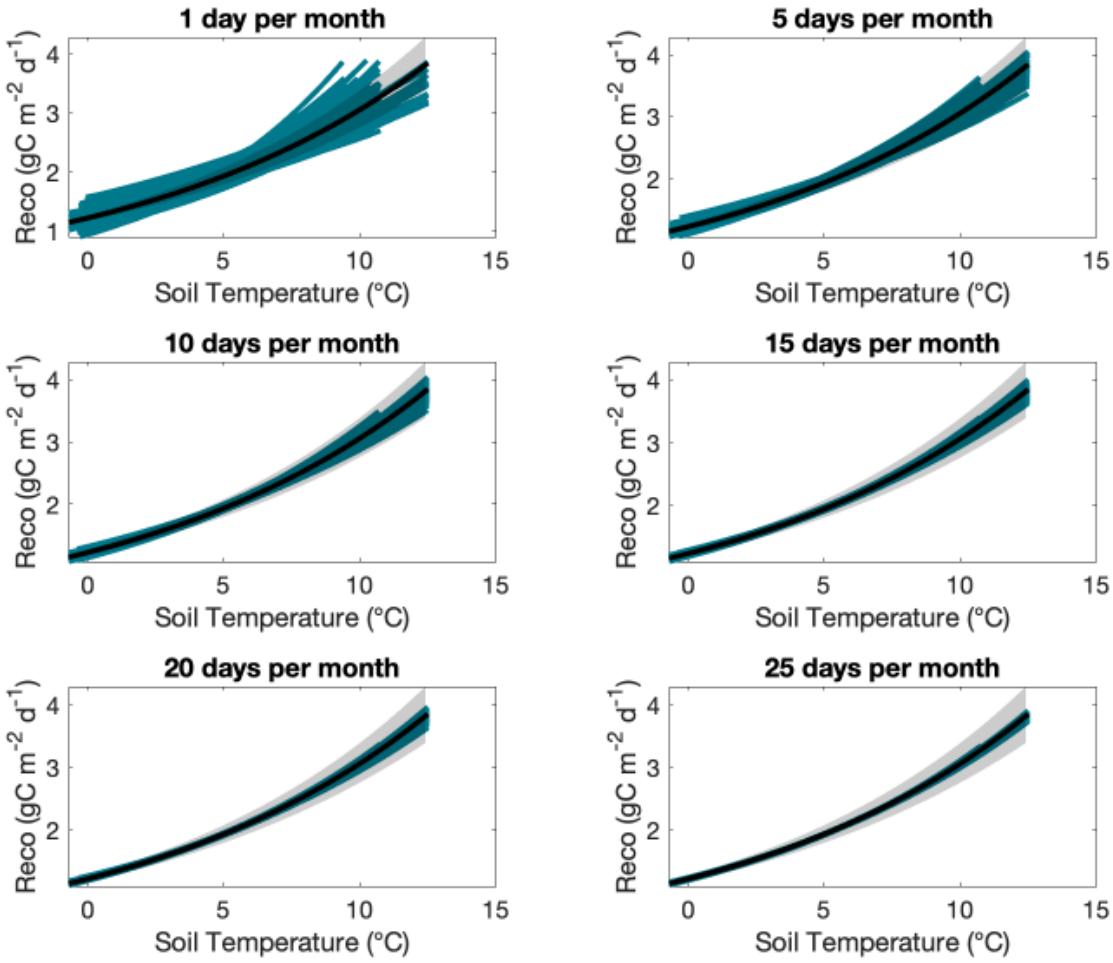


Figure S5. Functional relationships at US-EML constructed with one daily measurement per month up to 30 daily measurements per month over the 2015-2019 measurement period. Each panel contains 500 colored lines, indicating 500 random iterations of selecting 1-30 days per month. The full functional relationship constructed with all daily measurements is indicated by a black line with its 95% CI shaded in gray.

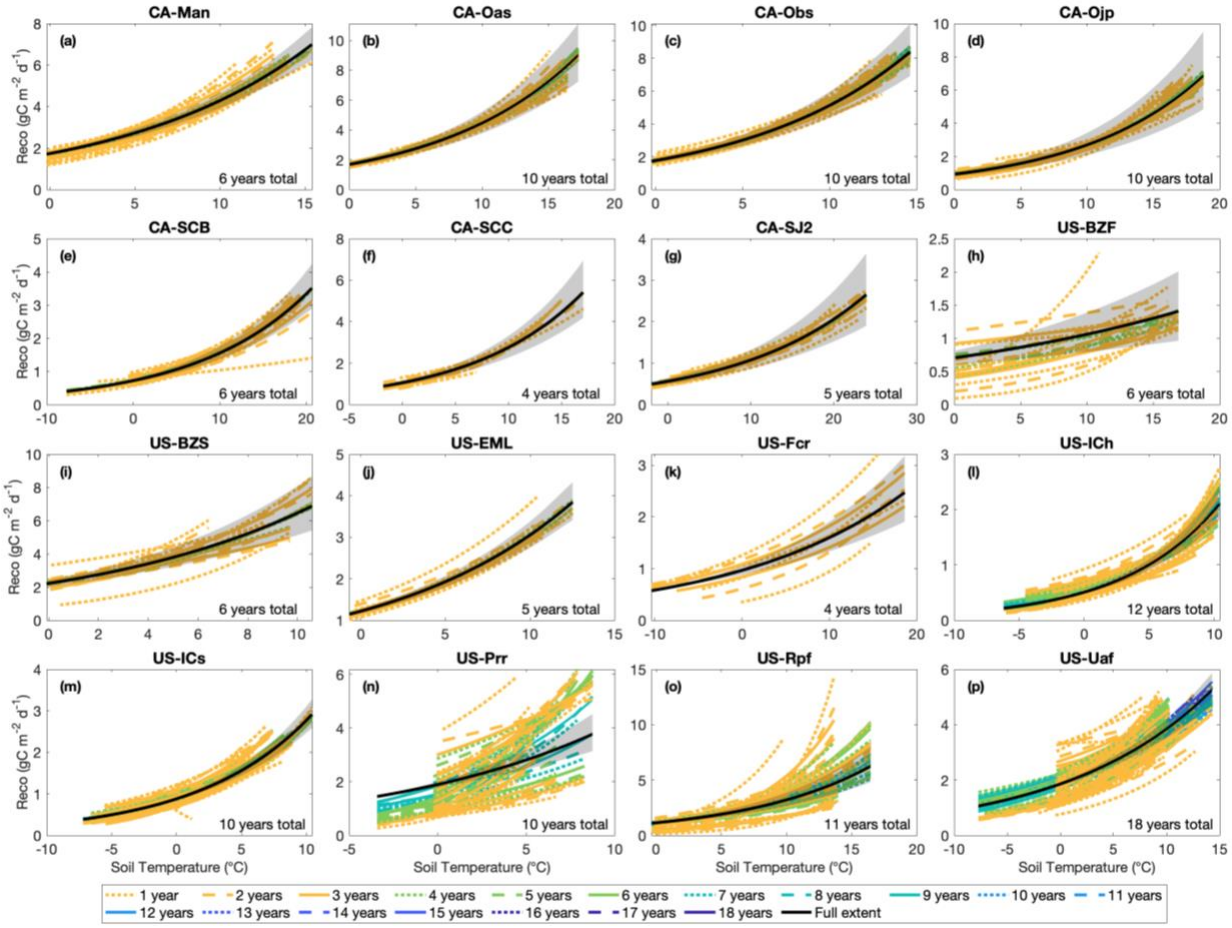


Figure S6. Impacts of temporal extent on the relationship between soil temperature and Reco at 16 flux tower sites. Black lines indicate the response of Reco to soil temperature calculated with daily data and the full temporal extent (ranging from 4 to 18 years depending on the site), with the shaded gray regions indicating the 95% CI. Colored lines indicate relationships created from all possible and consecutive subsets of temporal extents, ranging from one year (lighter colors) to 18 years (darker colors). Note that soil temperature and Reco are on different scales at each site.

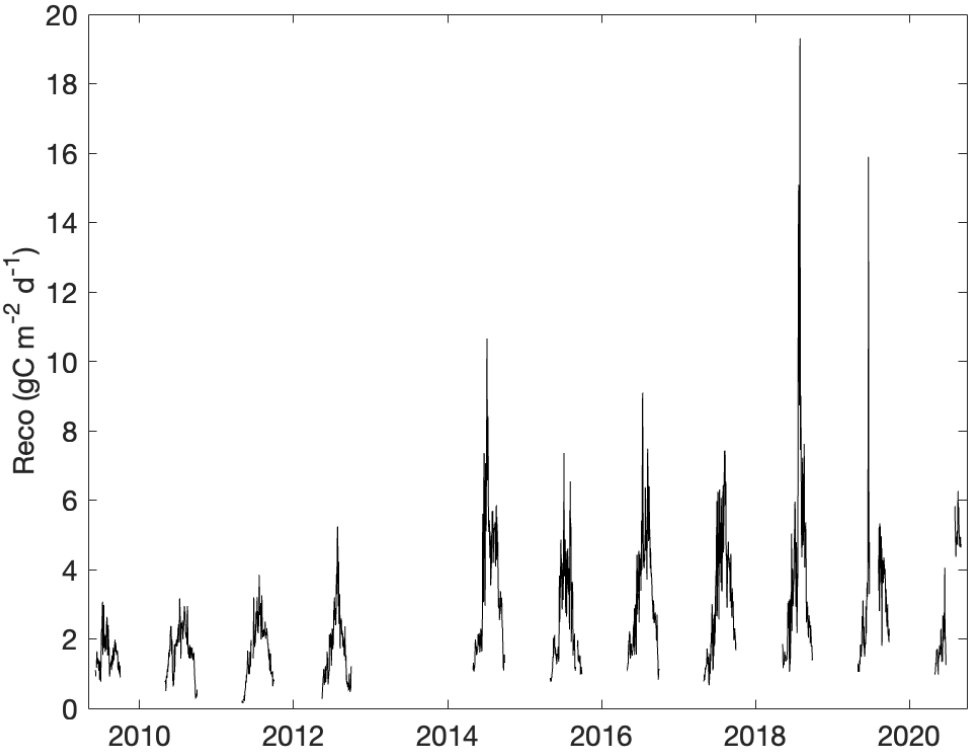


Figure S7. Daily mean Reco at the US-Rpf flux tower site from 2009-2020 following the 2004 wildfire. Reco measurements were subset over the growing season when soil temperature measurements at 5 cm depth were available.

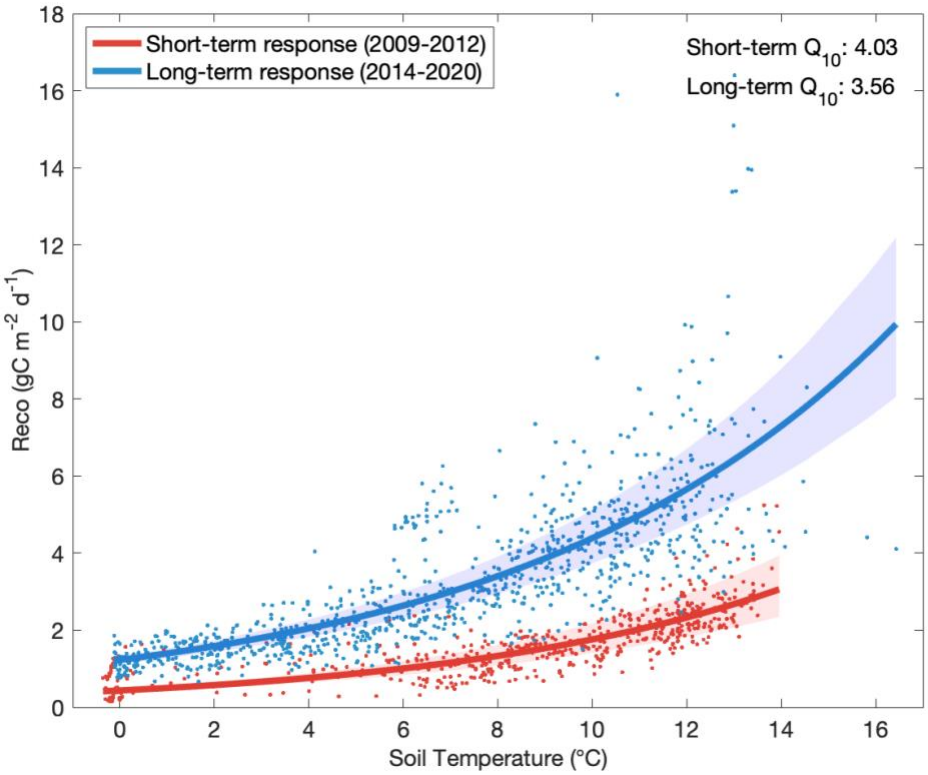


Figure S8. Functional relationships at US-Rpf separated by the short-term response after the wildfire (2009-2012) in red and the long-term response (2014-2020) in blue. Dots indicate daily mean measurements and shaded regions indicate the 95% CI of the exponential fit.

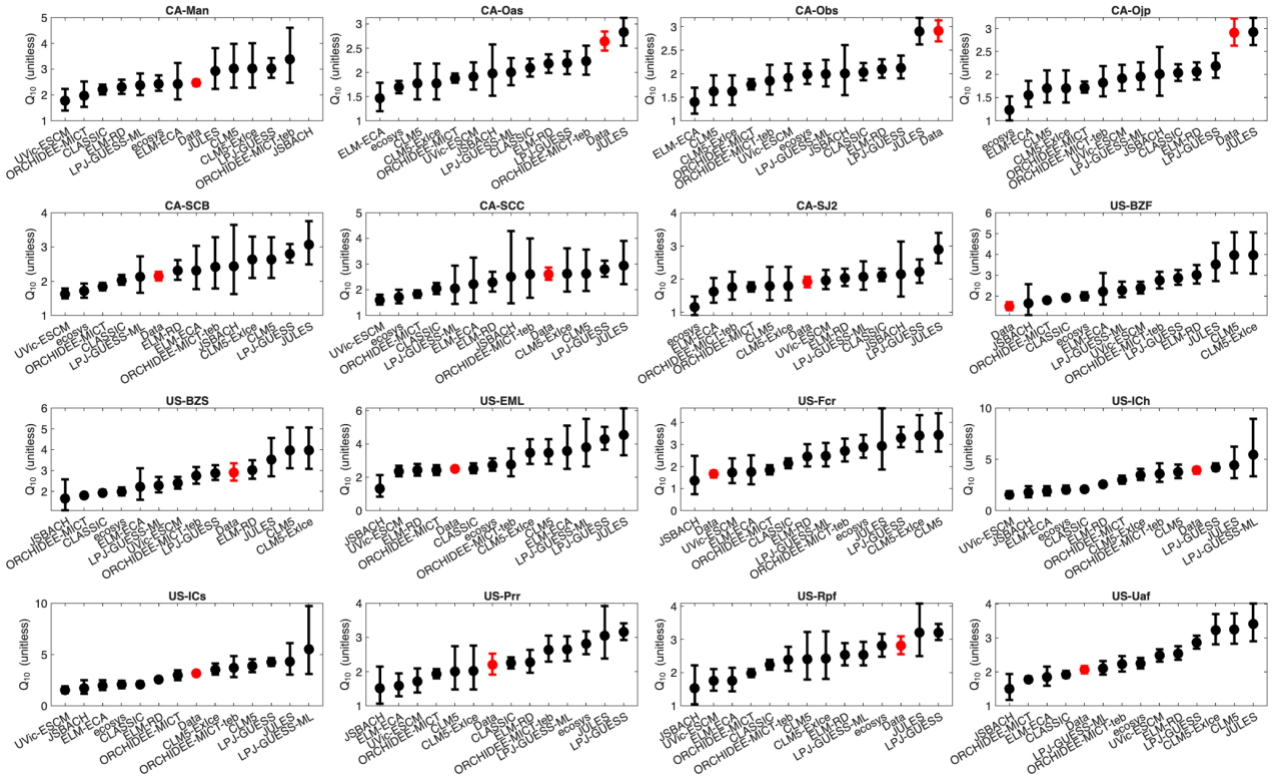


Figure S9. Apparent Q_{10} values for each model (black dots) and data (red dot) at the location of each flux tower. Error bars represent the 95% CI of each Q_{10}.

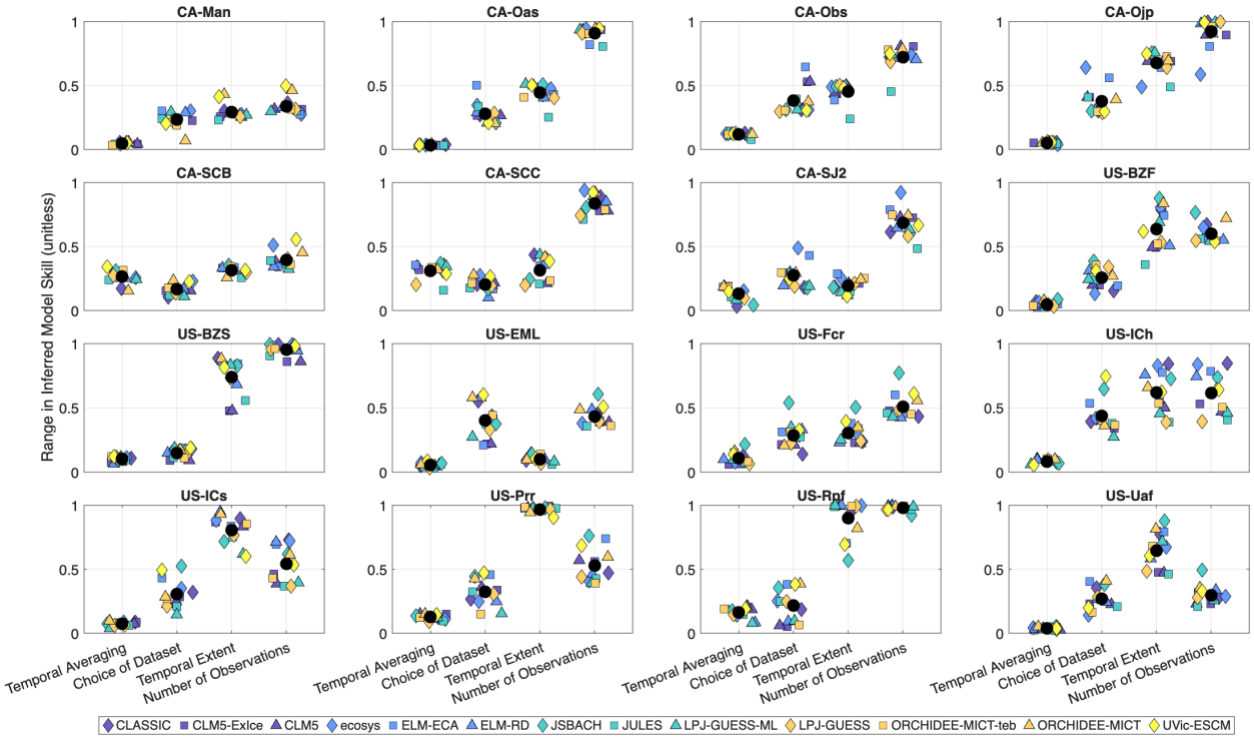


Figure S10. Range in inferred model skill through the Q_{10} scoring metric at each of the 16 flux tower sites. Inferred model skill scores vary according to benchmarking choices for temporal averaging, choice of dataset, temporal extent, and number of daily observations. Black dots indicate the mean range in inferred model skill for each category.

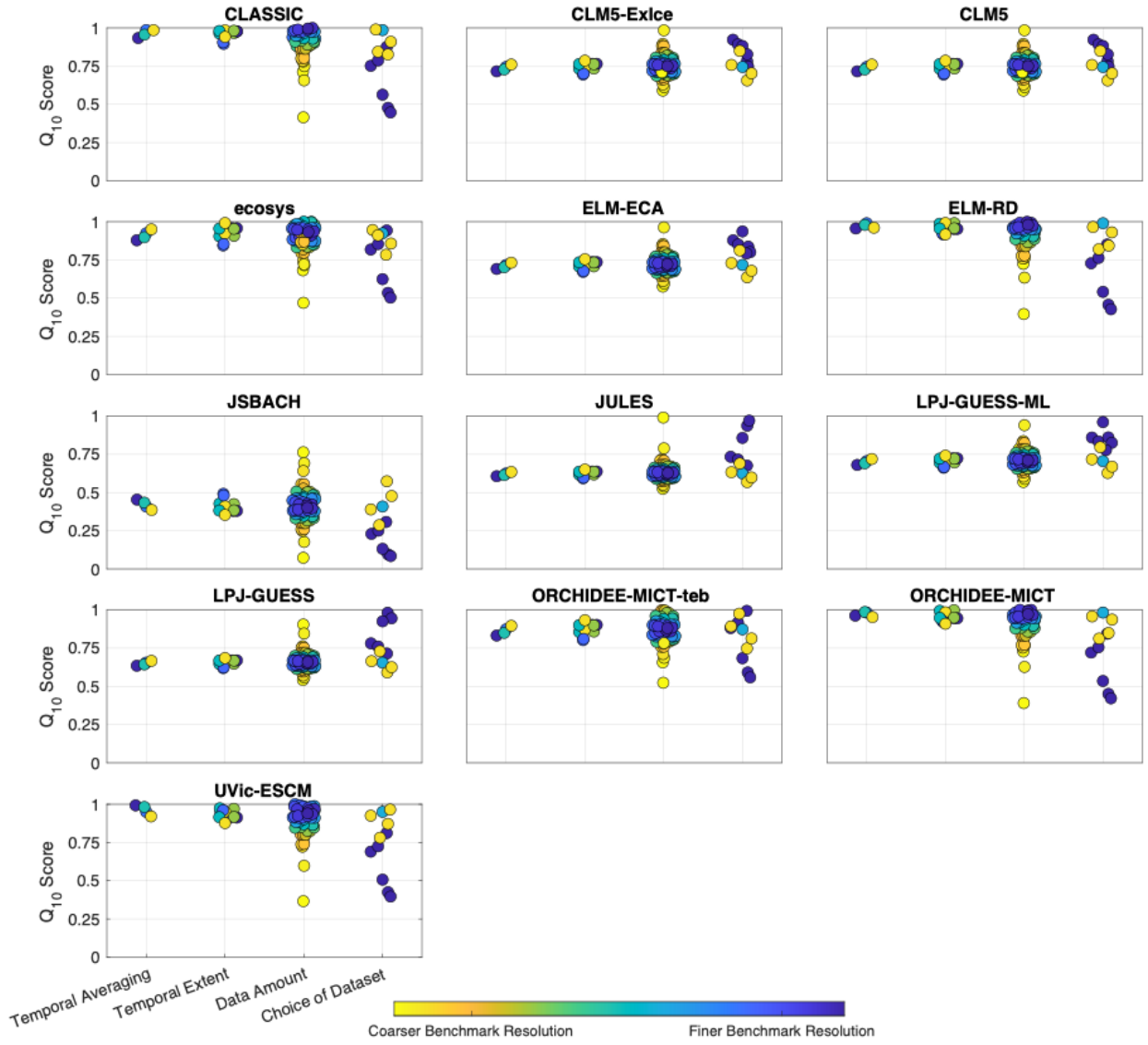


Figure S11. Impacts on inferred model skill at US-EML due to benchmarking choices for temporal averaging, temporal extent, number of daily observations, and choice of dataset through the Q_{10} scoring metric. Scores calculated from benchmarks with coarser temporal and spatial resolutions and lower temporal extent are colored in yellow. Scores calculated from benchmarks with the finest resolution and most data available are colored in dark blue.

Table S1. Benchmarking choice categories and permutations applied to evaluate functional relationships.

Benchmarking choice	Permutation	Dataset(s) evaluated	Temporal resolution
Choice of dataset	Chamber scale	CiPEHR	Daily
	Flux tower scale	16 flux towers	Daily
	Gridded scale	FLUXCOMX x ERA-5	Monthly
	Gridded scale	FLUXCOMX x MERRA-2	Monthly
	Gridded scale	Virkkala 2024 x ERA-5	Monthly
	Gridded scale	Virkkala 2024 x MERRA-2	Monthly
Number of daily observations	1 - 30 days per month	16 flux towers	Daily
Temporal extent	1 year up to 18 years	16 flux towers	Daily
Temporal averaging	Half-hourly	16 flux towers	Half-hourly
	Daily	16 flux towers	Daily
	Weekly	16 flux towers	Weekly
	Monthly	16 flux towers	Monthly
	Seasonal	16 flux towers	Seasonal
Spatial Variation	-	16 flux towers	Daily

Table S2. Gridded data products used to assess impacts of choice of dataset on apparent Q_{10}.

Data product	Variable	Spatial resolution	Temporal resolution	Temporal coverage	Data type	Reference
Virkkala 2024	Reco	1-km	Monthly	2001-2020	Upscaled machine learning	Virkkala et al. 2024
FLUXCOM-X	Reco	0.5° × 0.5°	Monthly	2001-2021	Upscaled machine learning	Nelson et al. 2023
ERA-5	Soil temperature	0.25° × 0.25°	Monthly	2001-2020	Global atmospheric reanalysis	ECMWF 2019
MERRA-2	Soil temperature	0.5° × 0.625°	Monthly	2001-2020	Global atmospheric reanalysis	GMAO 2015

Table S3. Models from WrPMIP that were used in the analysis.

Model	Native spatial resolution	Temporal coverage	Reference
CLASSIC	1.0° × 1.0°	2000-2021	Melton et al. (2020)
CLM5.0	0.5° × 0.5°	2001-2021	Lawrence et al. (2019)
CLM5-ExIce	0.5° × 0.5°	2001-2021	Lee et al. (2014)
ecosys	0.5° × 0.5°	2000-2021	Grant et al. (2015); Grant et al. (2017)
ELM-ECA	0.5° × 0.5°	2000-2021	Zhu et al. (2019)
ELM-RD	0.5° × 0.5°	2000-2021	Zhu et al. (2019); Burrows et al. (2020)
JSBACH	1.85° × 1.85°	2000-2021	Reick et al. (2021)
JULES	0.5° × 0.5°	2000-2022	Burke et al. (2017); Chadburn et al. (2017); Wiltshire et al. (2020)
LPJ-GUESS	0.5° × 0.5°	2000-2021	Smith et al. (2014); Pongracz et al. (2021)
LPJ-GUESS-ML	0.5° × 0.5°	2000-2021	Smith et al. (2014); Pongracz et al. (2021)
ORCHIDEE-MICT	0.5° × 0.5°	2000-2021	Guimberteau et al. (2018)
ORCHIDEE-MICT-teb	0.5° × 0.5°	2000-2021	Xi et al. (2024)
UVic-ESCM	1.8° × 1.8°	2000-2021	MacDougall et al. (2012); Mengis et al. (2020)

Table S4. Functional relationship permutations applied as benchmarks to evaluate the range in inferred model skill.

Benchmarking choice category	Dataset(s) applied as benchmarks	Permutation
Choice of dataset	Chambers, flux towers, upscaled datasets	Full dataset (daily data for chamber and flux tower, monthly for upscaled)
Data amount	Flux towers	Minimum and maximum Q_{10} from 500 random iterations of 1 through 30 days per month
Temporal extent	Flux towers	Minimum and maximum Q_{10} for 1 year subsets up to full time period
Temporal averaging	Flux towers	Half-hourly, daily, weekly, monthly

Table S5. Apparent Q_{10} values with the 95% CI in brackets, R^2 value of the functional relationship, and number of observations (n) at each flux tower site when using half-hourly,

daily, weekly, monthly, and seasonally averaged data. An * denotes sites where n = 5 or less, or where physically improbable Q_{10} values were > 25 and were manually excluded.

	Half-hourly	Daily	Weekly	Monthly	Seasonal
CA-Man					
Q_{10} [95% CI]:	2.51 [2.47, 2.55]	2.47 [2.36, 2.58]	2.58 [2.31, 2.88]	2.61 [2.08, 3.29]	1.54 [0.66, 3.58]
R^2:	0.54	0.69	0.74	0.77	0.32
n:	14711	873	133	30	6
CA-Oas					
Q_{10} [95% CI]:	2.57 [2.5, 2.65]	2.64 [2.45, 2.84]	2.66 [2.39, 2.97]	2.57 [2.11, 3.13]	2.68 [1.1, 6.52]
R^2:	0.29	0.42	0.66	0.71	0.45
n:	12416	1249	225	50	10
CA-Obs					
Q_{10} [95% CI]:	2.96 [2.87, 3.06]	2.9 [2.69, 3.14]	3.03 [2.72, 3.37]	2.65 [2.23, 3.15]	3.67 [0.87, 15.4]
R^2:	0.48	0.54	0.74	0.79	0.35
n:	6917	911	223	50	10
CA-Ojp					
Q_{10} [95% CI]:	2.77 [2.65, 2.9]	2.91 [2.62, 3.22]	2.95 [2.63, 3.31]	2.83 [2.44, 3.3]	1.28 [0.76, 2.14]
R^2:	0.29	0.37	0.70	0.85	0.13
n:	7250	1038	220	50	10
CA-SCB					
Q_{10} [95% CI]:	1.5 [1.48, 1.51]	2.15 [2.03, 2.27]	2.41 [2.09, 2.78]	2.52 [1.84, 3.44]	7.13 [2.24, 22.75]
R^2:	0.25	0.55	0.63	0.64	0.88
n:	17163	738	115	28	6
CA-SCC					
Q_{10} [95% CI]:	2.52 [2.41, 2.64]	2.61 [2.38, 2.86]	3.14 [2.67, 3.69]	3.68 [2.92, 4.64]	*
R^2:	0.39	0.56	0.82	0.94	*
n:	2918	427	66	15	4
CA-SJ2					
Q_{10} [95% CI]:	1.99 [1.92, 2.06]	1.91 [1.76, 2.08]	2.31 [2.01, 2.66]	2.28 [1.82, 2.85]	*
R^2:	0.28	0.34	0.64	0.76	*
n:	3903	537	99	23	5
US-BZF					
Q_{10} [95% CI]:	1.34 [1.28, 1.39]	1.51 [1.33, 1.71]	1.44 [1.1, 1.88]	1.36 [0.82, 2.26]	0.24 [0.02, 3.78]
R^2:	0.02	0.05	0.06	0.06	0.3
n:	10805	899	134	30	6
US-BZS					
Q_{10} [95% CI]:	3.24 [3.1, 3.37]	2.91 [2.52, 3.35]	3.03 [2.17, 4.22]	2.86 [1.47, 5.54]	1.43 [0.12, 17.26]
R^2:	0.27	0.22	0.27	0.29	0.04
n:	9158	890	136	30	6
US-EML					
Q_{10} [95% CI]:	2.36 [2.3, 2.43]	2.5 [2.35, 2.66]	2.42 [2.13, 2.75]	2.58 [2, 3.32]	*
R^2:	0.32	0.61	0.69	0.76	*
n:	7402	631	102	24	5
US-Fcr					
Q_{10} [95% CI]:	1.76 [1.72, 1.81]	1.66 [1.51, 1.81]	1.57 [1.23, 2]	1.42 [0.81, 2.5]	*
R^2:	0.21	0.19	0.16	0.1	*
n:	7078	576	87	20	4
US-Ich					

Q_{10} [95% CI]:	4.19 [4.07, 4.32]	3.92 [3.6, 4.27]	3.78 [3.12, 4.58]	3.93 [2.76, 5.6]	3.15 [0.52, 19.19]
R^2:	0.44	0.52	0.52	0.59	0.2
n:	11542	1096	211	55	12
US-Ics					
Q_{10} [95% CI]:	3.23 [3.15, 3.31]	3.15 [2.93, 3.4]	3.16 [2.67, 3.74]	3.47 [2.64, 4.58]	*
R^2:	0.44	0.54	0.54	0.71	*
n:	10276	889	173	45	10
US-Prr					
Q_{10} [95% CI]:	2.56 [2.46, 2.66]	2.2 [1.9, 2.53]	2.25 [1.56, 3.24]	2.27 [1, 5.15]	*
R^2:	0.11	0.09	0.09	0.09	*
n:	18145	1373	213	48	10
US-Rpf					
Q_{10} [95% CI]:	2.93 [2.85, 3.02]	2.82 [2.56, 3.1]	2.77 [2.22, 3.46]	2.37 [1.54, 3.65]	0.31 [0.08, 1.13]
R^2:	0.27	0.29	0.33	0.29	0.33
n:	18425	1499	229	52	11
US-Uaf					
Q_{10} [95% CI]:	2.12 [2.09, 2.16]	2.07 [1.96, 2.18]	2.07 [1.83, 2.34]	2.02 [1.56, 2.6]	1.71 [0.25, 11.51]
R^2:	0.19	0.23	0.28	0.28	0.02
n:	37222	2635	398	89	18

Table S6. Model scores for each WrPMIP model when benchmarked against daily observations from each flux tower. Scores range from 0 to 1 and indicate the level of agreement between the Q_{10} calculated from the model and the Q_{10} calculated from observations.

	CA-Man	CA-Oas	CA-Obs	CA-Ojp	CA-SCB	CA-SCC	CA-SJ2	US-BZF	US-BZS	US-EML	US-Fcr	US-Ich	US-Ics	US-Prr	US-Rpf	US-Uaf
CLASSIC	0.88	0.82	0.79	0.79	0.79	0.80	0.83	0.74	0.74	0.99	0.84	0.82	0.82	0.89	0.89	0.74
CLM5-ExIce	0.84	0.66	0.58	0.63	0.95	0.95	0.68	0.69	0.69	0.76	0.77	0.75	0.74	0.79	0.97	0.80
CLM5	0.84	0.66	0.58	0.62	0.95	0.95	0.68	0.69	0.69	0.76	0.76	0.72	0.70	0.78	0.96	0.80
ecosys	0.97	0.62	0.77	0.36	0.63	0.63	0.31	0.78	0.78	0.92	0.88	0.80	0.81	0.89	0.90	0.90
ELM-ECA	0.97	0.49	0.46	0.54	0.92	0.88	0.58	0.88	0.88	0.74	0.64	0.72	0.76	0.56	0.66	0.70
ELM-RD	0.92	0.86	0.82	0.81	0.92	0.91	0.79	0.84	0.84	0.97	0.98	0.97	0.98	0.91	0.99	0.98
JSBACH	NA	0.77	0.78	0.78	0.97	1.00	0.85	0.61	0.61	0.41	0.43	0.65	0.64	0.52	0.52	0.51
JULES	0.87	0.89	0.87	0.87	0.83	0.86	0.87	0.75	0.75	0.64	0.86	0.65	0.66	0.84	0.80	0.76
LPJ-GUESS-ML	0.95	0.78	0.77	0.75	0.84	0.81	0.81	0.91	0.91	0.71	0.99	0.58	0.58	0.95	0.98	0.83
LPJ-GUESS	0.84	0.87	0.84	0.86	0.90	0.90	0.88	0.88	0.88	0.66	0.79	0.67	0.66	0.81	0.80	0.88
ORCHIDEE-MICT-teb	0.77	0.89	0.70	0.69	0.97	0.96	0.65	0.92	0.92	0.90	0.93	0.74	0.73	0.95	0.96	0.88
ORCHIDEE-MICT	0.76	0.72	0.66	0.63	0.70	0.69	0.65	0.67	0.67	0.97	0.70	0.85	0.86	0.74	0.77	0.67
UVic-ESCM	0.66	0.73	0.73	0.73	0.58	0.57	0.76	0.96	0.96	0.94	0.64	0.53	0.52	0.63	0.65	0.99

References

Burke, E. J., Chadburn, S. E., & Ekici, A. (2017). A vertical representation of soil carbon in the JULES land surface scheme (vn4.3-permafrost) with a focus on permafrost regions. *Geoscientific Model Development*, *10*(2), 959–975. https://doi.org/10.5194/gmd-10-959-2017

Burrows, S. M., Maltrud, M., Yang, X., Zhu, Q., Jeffery, N., Shi, X., Ricciuto, D., Wang, S., Bisht, G., Tang, J., Wolfe, J., Harrop, B. E., Singh, B., Brent, L., Baldwin, S., Zhou, T.,

Cameron-Smith, P., Keen, N., Collier, N., … Leung, L. R. (2020). The DOE E3SM v1.1 Biogeochemistry Configuration: Description and Simulated Ecosystem-Climate Responses to Historical Changes in Forcing. *Journal of Advances in Modeling Earth Systems*, *12*(9). https://doi.org/10.1029/2019MS001766

Chadburn, S. E., Krinner, G., Porada, P., Bartsch, A., Beer, C., Belelli Marchesini, L., Boike, J., Ekici, A., Elberling, B., Friborg, T., Hugelius, G., Johansson, M., Kuhry, P., Kutzbach, L., Langer, M., Lund, M., Parmentier, F. J. W., Peng, S., Van Huissteden, K., … Burke, E. J. (2017). Carbon stocks and fluxes in the high latitudes: Using site-level data to evaluate Earth system models. *Biogeosciences*, *14*(22), 5143–5169. https://doi.org/10.5194/bg-14-5143-2017

European Centre for Medium-Range Weather Forecasts (ECMWF). (2019). ERA5 Reanalysis (0.25 Degree Latitude-Longitude Grid) [Dataset]. Research Data Archive at the National Center for Atmospheric Research, Computational and Information Systems Laboratory. https://doi.org/10.5065/BH6N-5N20

Global Modeling and Assimilation Office (GMAO). (2015). MERRA-2 tavgM_2d_Ind_Nx: 2d,Monthlymean,Time-Averaged,Single-Level,Assimilation,Land Surface Diagnostics V5.12.4 [Dataset]. Greenbelt, MD, USA, Goddard Earth Sciences Data and Information Services Center (GES DISC). https://doi.org10.5067/8S35XF81C28F

Grant, R. F., Humphreys, E. R., & LaFleur, P. M. (2015). Ecosystem CO2 and CH4 exchange in a mixed tundra and a fen within a hydrologically diverse Arctic landscape: 1. Modeling versus measurements. *Journal of Geophysical Research: Biogeosciences*, *120*(7), 1366–1387. https://doi.org/10.1002/2014JG002888

Grant, R. F., Mekonnen, Z. A., Riley, W. J., Wainwright, H. M., Graham, D., & Torn, M. S. (2017). Mathematical Modelling of Arctic Polygonal Tundra with Ecosys: 1. Microtopography Determines How Active Layer Depths Respond to Changes in Temperature and Precipitation. *Journal of Geophysical Research: Biogeosciences*, *122*(12), 3161–3173. https://doi.org/10.1002/2017JG004035

Guimberteau, M., Zhu, D., Maignan, F., Huang, Y., Yue, C., Dantec-N d lec, S., Ottl, C., Jornet-Puig, A., Bastos, A., Laurent, P., Goll, D., Bowring, S., Chang, J., Guenet, B., Tifafi, M., Peng, S., Krinner, G., Ducharne, A. s., Wang, F., … Ciais, P. (2018). ORCHIDEE-MICT (v8.4.1), a land surface model for the high latitudes: model description and validation. *Geoscientific Model Development*, *11*(1), 121–163. https://doi.org/10.5194/gmd-11-121-2018

Lawrence, D. M., Fisher, R. A., Koven, C. D., Oleson, K. W., Swenson, S. C., Bonan, G., Collier, N., Ghimire, B., van Kampenhout, L., Kennedy, D., Kluzek, E., Lawrence, P. J., Li, F., Li, H., Lombardozzi, D., Riley, W. J., Sacks, W. J., Shi, M., Vertenstein, M., … Zeng, X. (2019). The Community Land Model Version 5: Description of New Features, Benchmarking, and Impact of Forcing Uncertainty. *Journal of Advances in Modeling Earth Systems*, *11*(12), 4245–4287. https://doi.org/10.1029/2018MS001583

Lee, H., Swenson, S. C., Slater, A. G., & Lawrence, D. M. (2014). Effects of excess ground ice on projections of permafrost in a warming climate. *Environmental Research Letters*, *9*(12). https://doi.org/10.1088/1748-9326/9/12/124006

MacDougall, A. H., Avis, C. A., & Weaver, A. J. (2012). Significant contribution to climate warming from the permafrost carbon feedback. *Nature Geoscience*, *5*(10), 719–721. https://doi.org/10.1038/ngeo1573

Melton, J. R., Arora, V. K., Wisernig-Cojoc, E., Seiler, C., Fortier, M., Chan, E., & Teckentrup, L. (2020). CLASSIC v1.0: The open-source community successor to the Canadian Land Surface Scheme (CLASS) and the Canadian Terrestrial Ecosystem Model (CTEM)-Part 1: Model framework and site-level performance. *Geoscientific Model Development*, *13*(6), 2825–2850. https://doi.org/10.5194/gmd-13-2825-2020

Mengis, N., Keller, D. P., Macdougall, A. H., Eby, M., Wright, N., Meissner, K. J., Oschlies, A., Schmittner, A., Macisaac, A. J., Damon Matthews, H., & Zickfeld, K. (2020). Evaluation of the University of Victoria Earth System Climate Model version 2.10 (UVic ESCM 2.10). *Geoscientific Model Development*, *13*(9), 4183–4204. https://doi.org/10.5194/gmd-13-4183-2020

Nelson, J. A., Walther, S., Jung, M., Gans, F., Kraft, B., Weber, U., Hamdi, Z., Duveiller, G., and Zhang, W. (2023). FLUXOM-X-BASE [Dataset]. ICOS. https://doi.org/10.18160/5NZG-JMJE

Pongracz, A., Wårlind, D., Miller, P. A., & Parmentier, F. J. W. (2021). Model simulations of arctic biogeochemistry and permafrost extent are highly sensitive to the implemented snow scheme in LPJ-GUESS. *Biogeosciences*, *18*(20), 5767–5787. https://doi.org/10.5194/bg-18-5767-2021

Reick, C., Gayler, V., Goll, D., Hagemann, S., Heidkamp, M., Nabel, J., et al. (2021). *JSBACH 3 – The land component of the MPI Earth System Model: Documentation of version 3.2* (Technical Report). MPI für Meteorologie.

Smith, B., Wärlind, D., Arneth, A., Hickler, T., Leadley, P., Siltberg, J., & Zaehle, S. (2014). Implications of incorporating N cycling and N limitations on primary production in an individual-based dynamic vegetation model. *Biogeosciences*, *11*(7), 2027–2054. https://doi.org/10.5194/bg-11-2027-2014

Wiltshire, A. J., Carolina Duran Rojas, M., Edwards, J. M., Gedney, N., Harper, A. B., Hartley, A. J., Hendry, M. A., Robertson, E., & Smout-Day, K. (2020). JULES-GL7: The Global Land configuration of the Joint UK Land Environment Simulator version 7.0 and 7.2. *Geoscientific Model Development*, *13*(2), 483–505. https://doi.org/10.5194/gmd-13-483-2020

Virkkala, A-M., B.M. Rogers, J.D. Watts, K. Arndt, S. Potter, I. Wargowsky, and S. Natali. 2024. Machine learning-based Arctic-boreal terrestrial ecosystem CO2 fluxes, 2001-2020 [Dataset]. ORNL DAAC, Oak Ridge, Tennessee, USA. https://doi.org/10.3334/ORNLDAAC/2377

Xi, Y., Qiu, C., Zhang, Y., Zhu, D., Peng, S., Hugelius, G., Chang, J., Salmon, E., & Ciais, P. (2024). Assessment of a tiling energy budget approach in a land surface model, ORCHIDEE-MICT (r8205). *Geoscientific Model Development*, *17*(12), 4727–4754. https://doi.org/10.5194/gmd-17-4727-2024

Zhu, Q., Riley, W. J., Tang, J., Collier, N., Hoffman, F. M., Yang, X., & Bisht, G. (2019). Representing Nitrogen, Phosphorus, and Carbon Interactions in the E3SM Land Model: Development and Global Benchmarking. *Journal of Advances in Modeling Earth Systems*, *11*(7), 2238–2258. https://doi.org/10.1029/2018MS001571